Integration of site-controlled pyramidal quantum dots and photonic crystal membrane cavities

P. Gallo,[1,a)] M. Felici,[1] B. Dwir,[1] K. A. Atlasov,[1] K. F. Karlsson,[1] A. Rudra,[1] A. Mohan,[1] G. Biasiol,[2] L. Sorba,[3] and E. Kapon[1]
[1]*Laboratory of Physics of Nanostructures, Ecole Polytechnique Fédérale de Lausanne (EPFL), CH-1015 Lausanne, Switzerland*
[2]*Laboratorio Nazionale TASC INFM-CNR, I-34012 Trieste, Italy*
[3]*NEST INFM-CNR and Scuola Normale Superiore, I-56126 Pisa, Italy*

(Received 2 May 2008; accepted 5 June 2008; published online 30 June 2008)

The authors demonstrate the deterministic coupling between a single, site-controlled InGaAs/GaAs pyramidal quantum dot (QD) and a photonic crystal membrane cavity defect. The growth of self-ordered pyramidal QDs in small (300 nm base side) tetrahedral recesses etched on (111)*B* GaAs substrates was developed in order to allow their integration within the thin GaAs membranes. Accurate (better than 50 nm) positioning of the QD with respect to the optical cavity mode is achieved reproducibly owing to the site control. Coupling of the dot emission with the cavity mode is evidenced in photoluminescence measurements. The deterministic positioning of the pyramidal QDs and the control of their emission spectrum opens the way for devices based on QDs integrated with coupled nanocavities. © *2008 American Institute of Physics*. [DOI: 10.1063/1.2952278]

Controlling the photon emission by manipulating the optical modes surrounding an emitter is one of the major challenges of current quantum photonic research. A useful approach for realizing such system is to integrate the emitter within a photonic crystal[1] (PhC) cavity, which would allow obtaining particularly high Purcell factors due to the high finesse and the small mode volumes achievable. Moreover, single or few quantum dot (QD) light sources integrated in such cavities would be attractive for numerous applications, including thresholdless nanolasers[2] and high-efficiency single-photon emitters.[3] One can also foresee the realization of quantum information devices using such cavity-QD systems.[4] Recent progress in this field includes the demonstration of high-Q nanocavities[5] as well as the observation of strong coupling between a self-assembled QD and a PhC defect cavity.[6,7] In Ref. 7, in particular, strong coupling could be achieved thanks to the development of a fabrication method allowing for the precise alignment of a PhC cavity with a single, preselected QD. However, further advancements will require the development of techniques for achieving close control on the spatial position and on the emission spectrum of QD arrays. In particular, precise site and spectral control will be indispensable for achieving photonic coupling of several QDs via a system of coupled nanocavities. This is difficult, if not impossible, to obtain with self-assembly techniques such as the Stranski–Krastanow (SK) QD growth, which suffer from random nucleation positions and broad size distributions.

Here, we present the deterministic integration of a site-controlled QD with a PhC microcavity. The virtually perfect site control and the narrow inhomogeneous broadening achieved with the pyramidal QD structures facilitate the design of the structure and the tuning of the QD emission into resonance with the optical cavity.

The InGaAs pyramidal QD structures were grown by organometallic chemical vapor deposition in nitrogen ambient on special membrane planar wafers grown by molecular beam epitaxy on undoped (111)*B* GaAs substrates. The membrane substrates consisted of a 1 μm thick AlGaAs layer of high aluminium content and of a 260 nm thick GaAs layer. The inverted pyramid patterns were made using electron beam lithography followed by wet chemical etching. The InGaAs/GaAs pyramidal QDs were subsequently self-formed at the tip of inverted pyramids etched onto (111)*B* GaAs substrates,[8] due to capillarity-induced surface fluxes of adatoms.[9] It has already been shown that the emission energy and the nucleation site of such pyramidal QDs can be closely controlled.[10]

In order to incorporate the pyramids inside the GaAs membrane layer, we investigated systematically the fabrication of such pyramidal QDs in small pyramids (<300 nm base side). The developed process involved a deoxidation temperature of ~570 °C prior to growth, which is about 100 °C below what is commonly employed. Hydrogen plasma has been demonstrated to be an efficient way to treat the samples before growth[11] (H is a strong reducing agent). Here, the native oxides present on the GaAs surface were removed by the reducing action of the hydrogen atoms released in the cracking of arsine. The low oxidation temperature dramatically reduces mass transport, and it helps in preserving the shallow substrate pattern. Moreover, since the QD has to be situated at the center of the GaAs membrane layer in order to provide efficient coupling with the cavity mode, QDs with thin (<50 nm thick) buffer layers were developed, without compromising their luminescence efficiency.

The evolution of the patterned (111)*B* GaAs surface during deoxidation and growth was investigated using *ex situ* atomic force microscopy (AFM). As an example, AFM images of a 500 nm pitch hexagonal array of inverted pyramids overgrown with a (nominally) 27 nm GaAs layer are shown in Fig. 1. In this particular case, the initial etched pyramids had 300 nm long base sides. The unetched (111)*B* surface surrounding the pyramidal recesses is known to exhibit neg-

a)Electronic mail: pascal.gallo@epfl.ch.

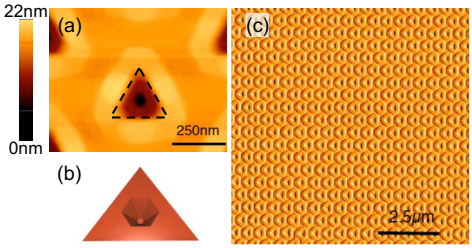

FIG. 1. (Color online) Arrays of site-controlled pyramids with a 300 nm base side, overgrown with a nominally 27 nm thick GaAs layer. (a) Top-view tapping mode AFM image of a single pyramid. The dashed lines indicate the initial boundaries of the pyramid. (b) Schematic illustration of the overgrown pyramid. (c) Top-view phase mode AFM image of a 500 nm pitch array of overgrown pyramids.

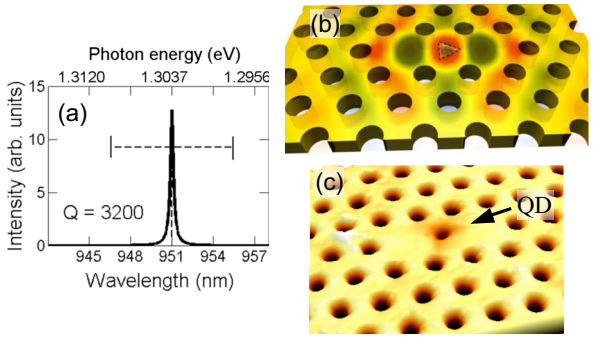

FIG. 2. (Color online) (a) Cavity response calculated via 3D FDTD numerical simulations. The horizontal dashed line represents the uncertainty on the wavelength of the cavity mode. The origin of this uncertainty lies in the experimental error (± 1 nm) associated with the measured values of r and a. (b) Schematic illustration of L_3 membrane cavity showing the pyramidal QD at its center. The calculated intensity electric field distribution of the confined mode is superposed. (c) AFM image of a pyramidal QD integrated in the PhC.

ligible growth rate due to the absence of effective decomposition of the metallorganic precursors on the As-rich facets. However, the AFM images clearly show growth of islands extending laterally on the (111)*B* surface from the edges of the pyramids, which serve as nucleation sites. This regular lateral growth is in contrast with the irregular, three-dimensional (3D) growth that takes place on an unpatterned (111)*B* substrate, yielding rough surfaces. The regular growth on the "no-growth" (111)*B* surface is important for achieving smooth membrane surfaces, and therefore for obtaining large cavity finesse values.

Most of the grown material, however, is deposited inside the pyramidal recesses, due to effective decomposition of the precursors at the (111)*A* Ga-rich facets [see Fig. 1(a)]. The growth rate is highest at these three facets, thus leading to a self-limiting growth in the tetrahedral inverted-pyramid template.[9] The small ratio between the (111)*A* and the (111)*B* no-growth areas leads to a rapid filling in of the pyramidal recess, which requires careful control of the growth rate to achieve the desired positioning of the QD within the membrane slab. Besides reducing the nominal growth rates by adjusting the flow rates of the precursors, we also introduced areas with micrometer-size etched pyramids on the substrate, around the area of interest, to avoid too large growth rates due to long-range (50–100 μm) diffusion of metallorganic precursors. We also note that the upper surface of the tetrahedral pyramid gradually acquires a hexagonal shape [see Figs. 1(a) and 1(b)]. This is because the dimensions of the base of the pyramid approach the size of the width of the facets produced between the (111)*A* facets due to capillarity. This size is determined by the diffusion length of the adatoms on the corresponding crystal facets,[9] and it is about 20–40 nm for the pyramidal structures. Thus, deposition of the GaAs buffer layer on the patterned (111)*B* substrate yields an array of regular hexagonal recesses due to the interplay of growth rate anisotropy and capillarity. Figure 1(c) shows an AFM image of such an array, attesting to the uniformity of such nanotemplate. Formation of the InGaAs QDs on this template proceeds by depositing a thin InGaAs layer, followed by a GaAs cap that can eventually planarize the upper surface almost completely.

The virtually perfect site control of the QDs is achieved by seeding the growth of each dot at a desired position, thanks to the preferential decomposition of the metallorganic precursors on the inner pyramid facets and the capillarity effect at the tip of the pyramid. Very good QD uniformity of such structures has already been demonstrated, with inhomogeneous broadening typically lower than 10 meV and as low as ~4 meV.[12] For the current studies, we produced also "single" QD structures, in which the pyramidal recesses were separated by several 10 μm in order to facilitate the fabrication of the PhC structure around them. These QDs are characterized by a good optical quality, evidenced by the small linewidth (<200 μeV) of the microphotoluminescence (micro-PL) peak associated with the single exciton. In addition, photon correlation experiments performed on similar QD structures have shown clear evidence of single photon emission,[13] a prerequisite for the observation of true quantum strong coupling between the QD and the PhC cavity.[6,7] Another important parameter for the determination of the QD-PhC coupling strength is the QD dipole moment, which can in turn be estimated from the QD size and radiative lifetime.[14] Regarding this point, it should be noted that both the size (~20 nm in the growth plane,[15] ~5 nm along the growth axis) and the lifetime [~1 ns (Ref. 13)] of our QDs are very similar to those measured for the SK dots employed to achieve strong coupling in other QD-PhC cavity systems.[6,7]

Based on the results of the AFM characterization and low temperature PL studies of similar structures, the QD layer structure for integration with the PhC cavity was designed and grown on the (111)*B* GaAs/AlGaAs membrane wafer patterned with pyramidal recesses of various patterns. The grown structure consisted of a 6.5 nm GaAs buffer layer, a 0.5 nm $Ga_{0.8}In_{0.2}As$ QD layer and a 20 nm GaAs cladding layer (all layers were nominally undoped). Thicknesses correspond to "nominal values," referring to measured values of layers grown simultaneously on (100) GaAs substrates. The emission spectra of the QDs were measured using a micro-PL setup in a helium flow cryostat using a ~1 μm spot of an Ar^+ laser at $\lambda = 514.5$ nm as the excitation source. Based on these measurements, a target QD emission wavelength of 930–950 nm was set. A PhC cavity consisting of an hexagonal array of cylindrical holes and incorporating an unmodified L_3 defect cavity was then designed with the aid of a 3D finite difference time domain (FDTD) simulation based on a standard Yee algorithm[16] [see Figs. 2(a) and 2(b)]. The Fourier transforms of the simulated signals were calculated using the Padé–Baker approximation,[17,18] allowing for an optimum ratio between the number of iterations and the

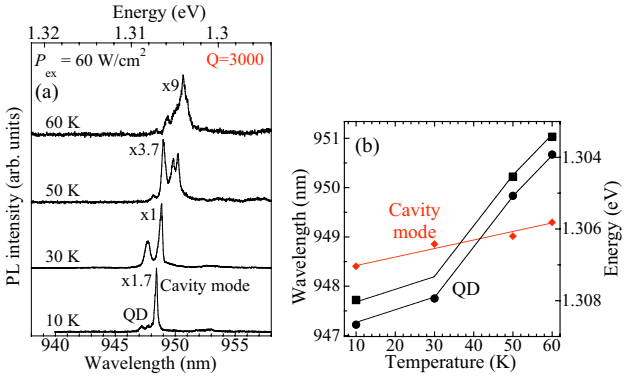

FIG. 3. (Color online) (a) Micro-PL spectra of the integrated QD-cavity structure acquired at several temperatures. (b) Temperature dependence of the wavelength of the "free" QD emission (black filled circles and squares) and of that of the observed cavity mode (red filled diamonds). The continuous lines are guides to the eye.

spectral resolution. From these simulations, it was obtained that the fundamental cavity mode (TE_0-like with respect to out-of-plane axis) overlaps with the QD emission spectrum for $a \sim 210$ nm and $r \sim 50$ nm, where a and r are the period and the hole radius, respectively.

The designed PhC cavities were then fabricated on top of the grown QD sample using electron beam lithography with high precision alignment[19] of polymethyl methacrylate deposited on top of 80 nm thick SiO_2 film patterned using CHF_3/Ar reactive ion etching. This layer was then used as a mask for inductively coupled plasma BCl_3/N_2 etching of the GaAs membrane layer.[20] The sacrificial AlGaAs layer was etched in diluted HF to release the membrane.

Figures 2(a) and 2(b) show the computed response function and near field pattern for the fundamental mode of a PhC cavity structure whose period and hole radius (a =211 nm, r=45 nm) were extrapolated from top-view and cross-section scanning electron microscope images of the cavity actually used in the experiments. An AFM image of such cavity (perfectly aligned with a pyramidal QD) is shown in Fig. 2(c). The wavelength of the computed cavity resonance [see Fig. 2(a)] is 951 ± 5 nm, where the ± 5 nm uncertainty originates from the experimental error (± 1 nm) associated with the measured values of r and a. A finesse value of Q=3200 is estimated from the linewidth of this resonance. This value can actually serve as a benchmark for the quality of the fabricated PhC structure [see Fig. 2(c)], since the experimental Q factor is expected to approach the computed one only for a nearly ideal PhC cavity.

Figure 3(a) shows the micro-PL spectra of the integrated QD cavity structure at several temperatures, all excited at 514.5 nm wavelength and 60 W/cm^2 power density (~ 1 μm spot size). For temperatures above ~ 50 K, the spectra correspond to "free" QD emission, at wavelengths >950 nm that do not match the cavity resonance. These spectra show typically several lines, corresponding to exciton complexes confined in the dot.[21] At lower temperatures, resonant coupling with the cavity mode at ~ 949 nm wavelength is evidenced. Within the uncertainty, the experimental value of the wavelength of the cavity mode matches the computed one (951 ± 5 nm). Figure 3(b) demonstrates that the temperature dependence of this spectral line is much weaker than that of the free QD spectral lines, reflecting the temperature variation of the refractive index of the cavity (24 μeV/K).[22] The spectral feature associated with the cavity resonance suggests a quality factor of ~ 3000, in very good agreement with the computed value of 3200. This confirms the good quality of the fabricated structure, and it suggests that the small residual nonplanarity (<20 nm) resulting from the incomplete filling up of the pyramid [see Fig. 2(c)] does not affect the properties of our PhC cavity.

In summary, we demonstrated the deterministic integration of a site-controlled pyramidal QD with a PhC L_3 defect cavity. Thanks to the ability to accurately control the position and the emission energy of these QDs, a matching between the emitter and the cavity optical mode could be readily obtained. In the near future, we plan to incorporate our QDs in PhC cavities having higher Q factors (i.e., with modified cavity terminations[5]), which should allow for the observation of strong coupling effects. However, our approach should be most useful for constructing more complex cavity QD systems, in which several dots are integrated with several, possibly coupled microcavities. Such structures would be useful for studies of photon-mediated exciton entanglement and very low threshold few-QD lasers.

[1] E. Yablonovitch, Phys. Rev. Lett. **58**, 2059 (1987).
[2] S. Noda, Science **314**, 206 (2006).
[3] D. Englund, D. Fattal, E. Waks, G. Solomon, B. Zhang, T. Nakaoka, Y. Arakawa, Y. Yamamoto, and J. Vuckovic, Phys. Rev. Lett. **95**, 013904 (2005).
[4] G. Khitrova, H. M. Gibbs, M. Kira, S. W. Koch, and A. Scherer, Nat. Phys. **2**, 81 (2006).
[5] Y. Akahane, T. Asano, B. S. Song, and S. Noda, Nature (London) **425**, 944 (2003).
[6] T. Yoshie, A. Scherer, J. Hendrickson, G. Khitrova, H. M. Gibbs, G. Rupper, C. Ell, O. B. Shchekin, and D. G. Deppe, Nature (London) **432**, 200 (2004).
[7] K. Hennessy, A. Badolato, M. Winger, D. Gerace, M. Atatüre, S. Gulde, S. Fält, E. L. Hu, and A. Imamoglu, Nature (London) **445**, 896 (2007).
[8] M. H. Baier, E. Pelucchi, E. Kapon, S. Varoutsis, M. Gallart, I. Robert-Philip, and I. Abram, Appl. Phys. Lett. **84**, 648 (2004).
[9] G. Biasiol and E. Kapon, Phys. Rev. Lett. **81**, 2962 (1998).
[10] E. Pelucchi, S. Watanabe, K. Leifer, Q. Zhu, B. Dwir, P. De Los Rios, and E. Kapon, Nano Lett. **7**, 1282 (2007).
[11] A. Callegari, P. D. Hoh, D. A. Buchanan, and D. Lacey, Appl. Phys. Lett. **54**, 332 (1989).
[12] K. Leifer, E. Pelucchi, S. Watanabe, F. Michelini, B. Dwir, and E. Kapon, Appl. Phys. Lett. **91**, 081106 (2007).
[13] A. Malko, D. Y. Oberli, M. H. Baier, E. Pelucchi, F. Michelini, K. F. Karlsson, M.-A. Dupertuis, and E. Kapon, Phys. Rev. B **72**, 195332 (2005).
[14] A. Thränhardt, C. Ell, G. Khitrova, and H. M. Gibbs, Phys. Rev. B **65**, 035327 (2002).
[15] Q. Zhu, E. Pelucchi, S. Dalessi, K. Leifer, M. A. Dupertuis, and E. Kapon, Nano Lett. **6**, 1036 (2006).
[16] A. Taflove and S. C. Hagness, *Computational Electrodynamics: The Finite-Difference Time-Domain Method* (Artech House, Boston, 2005).
[17] W. H. Guo, W. J. Li, and Y. Z. Huang, IEEE Microw. Wirel. Compon. Lett. **11**, 223 (2001).
[18] M. Qiu, Microwave Opt. Technol. Lett. **45**, 381 (2005).
[19] K. A. Atlasov, K. F. Karlsson, E. Deichsel, A. Rudra, B. Dwir, and E. Kapon, Appl. Phys. Lett. **90**, 153107 (2007).
[20] J. W. Lee, M. W. Devre, B. H. Reelfs, D. Johnson, J. N. Sasserath, F. Clayton, D. Hays, and S. J. Pearton, J. Vac. Sci. Technol. A **18**, 1220 (2000).
[21] K. F. Karlsson, V. Troncale, D. Y. Oberli, A. Malko, E. Pelucchi, A. Rudra, and E. Kapon, Appl. Phys. Lett. **89**, 251113 (2006).
[22] D. G. Gevaux, A. J. Bennett, R. M. Stevenson, A. J. Shields, P. Atkinson, J. Griffiths, D. Anderson, G. A. C. Jones, and D. A. Ritchie, Appl. Phys. Lett. **88**, 131101 (2006).